PROCEEDINGS OF SCIENCE

An investigation of different unintegrated parton distribution functions

Z. Badieian Baghsiyahi[a,*] **and M. Modarres**[b]

[a] *Department of Physics, University of Tehran, Tehran 1439955961, Iran*
[b] *Department of Physics, University of Tehran, Tehran 1439955961, Iran*

E-mail: zahra.badieian@ut.ac.ir, mmodares@ut.ac.ir

We investigate unintegrated parton distribution functions (UPDFs) by using the Kimber, Martin and Ryskin (KMR) and leading-order Martin, Ryskin and Watt (LOMRW) methods and compare them with transverse momentum dependent PDFs from the parton branching (PB) approach. The UPDFs are computed for various partons over a range x, μ^2, and k_t, revealing that all methods yield similar results at small values of k_t, while at higher k_t, the LOMRW UPDFs remain larger and the PB distributions decrease more rapidly. We then compute the reduced cross section (RCS) in deep inelastic scattering at $Q^2 = 4.5$ and $12 GeV^2$, finding that KMR and LOMRW predictions are consistent with PB results and experimental data at mid-x, though they overestimate the data at small x due to omission of the longitudinal structure function F_L.

QCD at the Extremes (QCDEX2025)
15 Sept 2025
Online

*Speaker

https://pos.sissa.it/

PoS(QCDEX2025)014

1. Introduction

The internal structure of hadrons in terms of their constituents quarks, antiquarks, and gluons remains a central topic in high-energy physics. The momentum distributions of these partons are encoded in the parton distribution functions (PDFs), $a(x, \mu^2)$, which describe the probability of finding a parton carrying a longitudinal momentum fraction x of the proton at a hard scale μ^2. Within the conventional collinear factorization framework, the PDFs evolve according to the DokshitzerGribovLipatovAltarelliParisi (DGLAP) equations [1–4]. In this approach, the transverse momentum k_t of partons is integrated out, leaving PDFs that depend only on x and μ^2. However, the transverse momentum of partons becomes crucial in the small-x regime and at high energies, where gluon dynamics dominate. These effects can be described by using transverse-momentum-dependent (TMD) or unintegrated parton distribution functions (UPDFs), denoted as $f_a(x, \mu^2, k_t^2)$. Unlike standard PDFs, UPDFs retain explicit dependence on k_t and therefore provide a more complete description of the initial-state kinematics. Several approaches have been developed to construct UPDFs. Among them, the KimberMartinRyskin (KMR) [5, 6] and MartinRyskinWatt (MRW) [7] prescriptions provide simple, leading-order (LO) methods to extend collinear PDFs into the k_t-dependent domain by implementing angular-ordering constraints (AOC) in the final evolution step. These approaches have been widely applied and tested against experimental data [8–13]. However, the parton branching (PB) method [14–16] generates TMDPDFs directly at next-to-leading order (NLO), including both x- and k_t-dependence throughout the evolution, and has shown excellent phenomenological performance. The aim of this work is to perform a systematic comparison of these approaches in order to identify their relative strengths and limitations. Specifically, we first generate UPDFs by using the KMR and LOMRW (LOMRW) methods for quarks, antiquarks, and gluons in terms of different values of x and μ^2. Then, we calculate the reduced cross section (RCS) in deep-inelastic scattering (DIS) at $Q^2 = 4.5$ and 12 GeV^2, and compare our results with those obtained by using the PB method as well as ZEUS experimental data. The structure of the paper is as follows. Section 2 describes the theoretical frameworks of KMR and LOMRW methods and the calculation of the reduced cross section. Section 3 presents discusses of our numerical results, including comparisons with PB predictions and experimental data. In conclusion, Section 4 summarizes our main findings and provides perspectives of our future work.

2. Theory

2.1 KMR and LOMRW Methods

As noted in the introduction, both the KimberMartinRyskin (KMR) and Martin, Ryskin and Watt (MRW) prescriptions are based on the DGLAP evolution equations, by using collinear PDFs, $a(x, \mu^2)$, and the leading-order (LO) splitting functions $P_{aa'}(x)$ as inputs. The essential idea is to extend these PDFs into the k_t -dependent domain by introducing angular-ordering constraints (AOC) in the last evolution step. For the KMR approach, the UPDFs for quarks and gluons are given by:

$$f_q(x,k_t^2,\mu^2) = T_q(k_t,\mu)\frac{\alpha_S(k_t^2)}{2\pi}\int_x^{1-\Delta} dz\left[P_{qq}(z)\frac{x}{z}q\left(\frac{x}{z},k_t^2\right)+P_{qg}(z)\frac{x}{z}g\left(\frac{x}{z},k_t^2\right)\right], \quad (1)$$

$$f_g(x,k_t^2,\mu^2) = T_g(k_t,\mu)\frac{\alpha_S(k_t^2)}{2\pi}\int_x^{1-\Delta} dz\left[P_{gq}(z)\frac{x}{z}\sum_q q\left(\frac{x}{z},k_t^2\right)+P_{gg}(z)\frac{x}{z}g\left(\frac{x}{z},k_t^2\right)\right], \quad (2)$$

where $a(x/z,k_t^2)$ are the integrated PDFs and $P_{ab}(z)$ are the LO splitting functions. To avoid soft-gluon singularities, a cutoff Δ is applied in the upper integration limit. Using the angular ordering condition (AOC) $\theta_{i+1} > \theta_i$, which implies $\mu > zk_t/(1-z)$, we derive the upper limit:

$$z_{\max} = \frac{\mu}{\mu + k_t}. \quad (3)$$

The Sudakov form factors $T_q(k_t,\mu)$ and $T_g(k_t,\mu)$ are given by:

$$T_q(k_t,\mu) = exp\left(-\int_{k_t^2}^{\mu^2}\frac{\alpha_S(k_t'^2)}{2\pi}\frac{dk_t'^2}{k_t'^2}C_F\left(-z_{max}-\frac{z_{max}^2}{2}-2\ln(1-z_{max})\right)\right), \quad (4)$$

$$T_g(k_t,\mu) = exp\left(-\int_{k_t^2}^{\mu^2}\frac{\alpha_S(k_t'^2)}{2\pi}\frac{dk_t'^2}{k_t'^2}\left\{2N_c\left(\frac{z_{max}^3}{3}-\frac{z_{max}^4}{4}-z_{max}^2-ln(1-z_{max})\right)\right.\right.$$
$$\left.\left.+\frac{n_f}{6}(3z_{max}-3z_{max}^2+2z_{max})\right\}\right). \quad (5)$$

The LOMRW method is similar in construction but applies the angular-ordering condition only to the terms that produce soft singularities. As a result, the LOMRW UPDFs for quarks and gluons are given by:

$$f_q(x,k_t^2,\mu^2) = T_q(k_t,\mu)\frac{\alpha_S(k_t^2)}{2\pi}\int_x^1 dz\left[P_{qq}(z)\frac{x}{z}q\left(\frac{x}{z},k_t^2\right)\Theta(z_{max}-z)+P_{qg}(z)\frac{x}{z}g\left(\frac{x}{z},k_t^2\right)\right], \quad (6)$$

and

$$f_g(x,k_t^2,\mu^2) = T_g(k_t,\mu)\frac{\alpha_S(k_t^2)}{2\pi}\int_x^1 dz\left[P_{gq}(z)\frac{x}{z}q\left(\frac{x}{z},k_t^2\right)+P_{gg}(z)\frac{x}{z}g\left(\frac{x}{z},k_t^2\right)\Theta(z_{max}-z)\right], \quad (7)$$

with the corresponding sudakov factors:

$$T_q(k_t,\mu) = exp\left(-\int_{k_t^2}^{\mu^2}\frac{\alpha_S(k_t'^2)}{2\pi}\frac{dk_t'^2}{k_t'^2}\int_0^{z_{max}} dz' P_{qq}(z')\right). \quad (8)$$

and

$$T_g(k_t,\mu) = exp\left(-\int_{k_t^2}^{\mu^2}\frac{\alpha_S(k_t'^2)}{2\pi}\frac{dk_t'^2}{k_t'^2}\left[\int_0^{z_{max}} dz' P_{gg}(z') + n_f\int_0^1 dz' P_{qg}(z')\right]\right), \quad (9)$$

Thus, while both KMR and LOMRW generate UPDFs by using collinear inputs, their main distinction lies in the treatment of the AOC and soft singularities, which in turn affects the large- k_t behavior of the distributions.

2.2 Reduced Cross Section

The reduced cross section in electron-proton deep inelastic scattering (DIS) is defined as:

$$\sigma_{\text{red}}(x, y, Q^2) = F_2(x, Q^2) - \frac{y^2}{1 + (1 - y)^2} F_L(x, Q^2), \tag{10}$$

where x is the Bjorken variable, y is the inelasticity, $Q^2 = -q^2$ is the hard scale, F_2 is the proton structure function, and F_L is the longitudinal structure function. As F_L is negligible for $y < 0.5$ [21], we omit it in our calculations.

3. Results and Discussions

3.1 KMR, LOMRW, and PB UPDFs

To understand the differences between the various methods, we first generated UPDFs by using the KMR and LOMRW prescriptions for quarks, antiquarks, and gluons at representative values of $x = 0.01$ and 0.0001 with the hard scale fixed at $\mu^2 = 1000$ GeV^2. The results are shown in Figs. 1,2. For comparison, we also include the PB TMDPDFs [14], plotted as $xA(x, k_t, \mu)$ versus k_t according to the TMDplotter convention: $f_a(x, k_t^2, \mu^2) = A(x, k_t, \mu)/k_t^2$. We observe that at small transverse momentum the KMR, LOMRW, and PB approaches yield similar results. However, as k_t increases, the LOMRW distributions become larger than those from KMR and PB, while the PB TMDPDFs decrease more rapidly and vanish at smaller k_t. This difference originates from the treatment of soft-gluon emissions: the absence of a cutoff for the q g splitting in LOMRW leads to enhanced distributions at large k_t. To further explore scale dependence, we generated UPDFs for the anti-up quark at $x = 0.01$ and two values of the hard scale, $Q^2 = \mu^2 = 10$, 100, and 1000 GeV^2 (3). For KMR and PB, the UPDFs at low k_t are larger for smaller scales, but the trend reverses at higher k_t. For LOMRW, however, the mid-scale ($\mu^2 = 100$ GeV^2) yields smaller UPDFs at low k_t, highlighting a distinct behavior compared to KMR and PB. In the PB approach, UPDFs vanish near the hard scale at low μ^2, but at higher scales they decrease earlier than expected, ultimately resembling KMR behavior. Overall, these comparisons confirm that while KMR and PB show qualitatively similar scale dependence, LOMRW tends to enhance distributions at large k_t, especially near the hard scale.

3.2 Reduced Cross Section

We next computed the reduced cross section for deep-inelastic scattering at $Q^2 = 4.5$ and 12 GeV^2 using MSHT20lo PDFs [22] to generate the corresponding UPDFs. The results are presented in Fig. **??** and compared to PB results from Ref. [14] (Fig. 4). Both KMR and LOMRW give nearly identical predictions across the full x range. At intermediate x, their results agree well with experimental data. At large x, however, both fall below the data since k_t-factorization is primarily valid at small x and high energy. At small x, the calculated cross sections overshoot the data, in contrast to expectations. This discrepancy can be traced to the omission of the longitudinal structure function F_L, which becomes significant for $x < 2.3 \times 10^{-4}$(corresponding to $y > 0.5$). By neglecting F_L, the cross section is artificially increased in this region. Despite this limitation, the reduced cross sections from KMR and LOMRW agree closely with PB results for both Q^2 values,

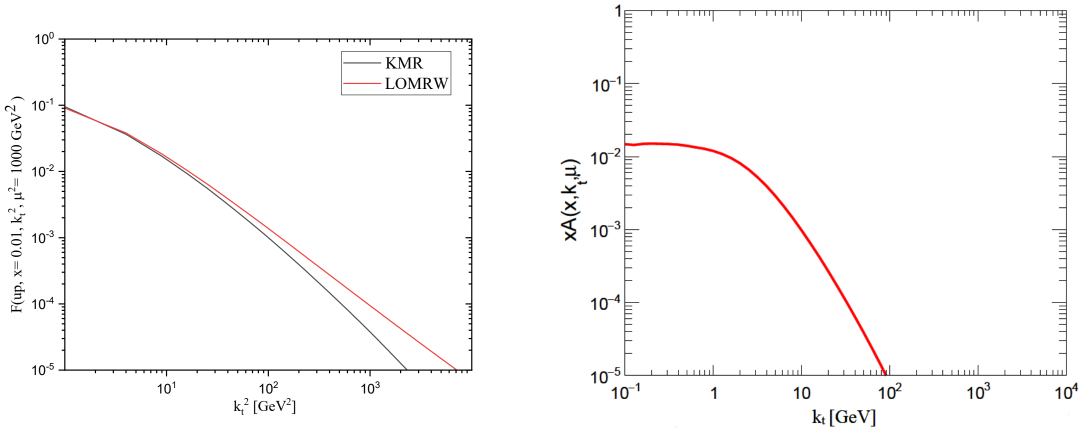

Figure 1: The UPDFs for up quark versus k_t^2 in $x = 0.01$ and $\mu^2 = 1000\ GeV^2$ for a) the KMR, LOMRW and b) PB method.

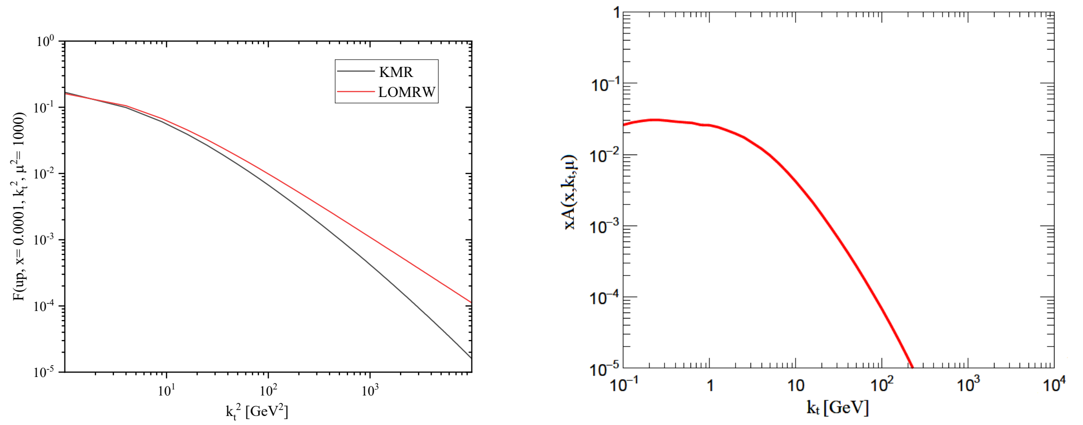

Figure 2: The UPDFs for the up quark versus k_t^2 in $x = 0.0001$ and $\mu^2 = 1000\ GeV^2$ for a) the KMR, LOMRW and b) PB methods.

diverging only at the smallest x. This suggests that the different approaches are consistent overall, with small discrepancies attributable to missing F_L contributions.

4. Conclusions

In this work, we generated UPDFs by using the KMR and LOMRW methods and compared them with the PB approach. We set $Q^2 = \mu^2$ in all calculations. At small k_t^2, all UPDFs agree well, but differences emerge at larger k_t, with LOMRW UPDFs being larger due to the absence of a cutoff in the qg splitting function. The KMR and PB UPDFs show similar behavior: at high k_t, UPDFs with larger hard scales are larger, while at low k_t and small hard scales, UPDFs are larger than those at higher hard scales. The LOMRW UPDFs are smaller at intermediate hard scales and low k_t.

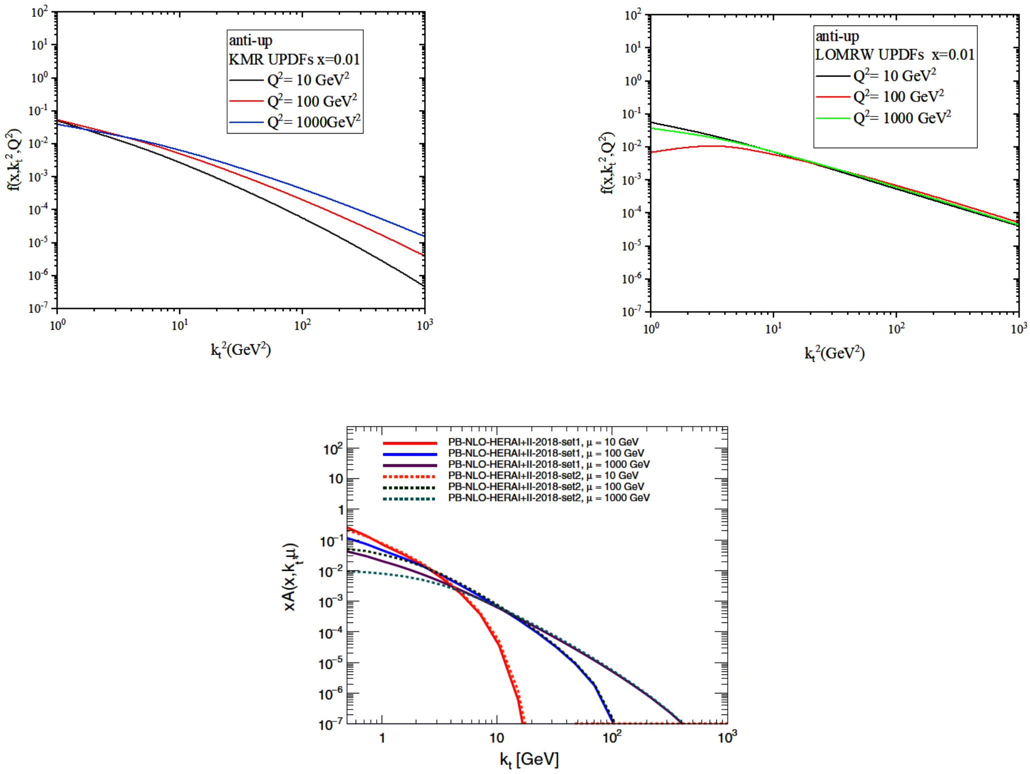

Figure 3: The UPDFs for anti-up quarks versus k_t^2 by a) KMR and b) MRW methods and c) and those of PB related to the reference [14] for $x = 0.01$ in $Q^2 = \mu^2 = 10$, 100 and 1000 GeV^2.

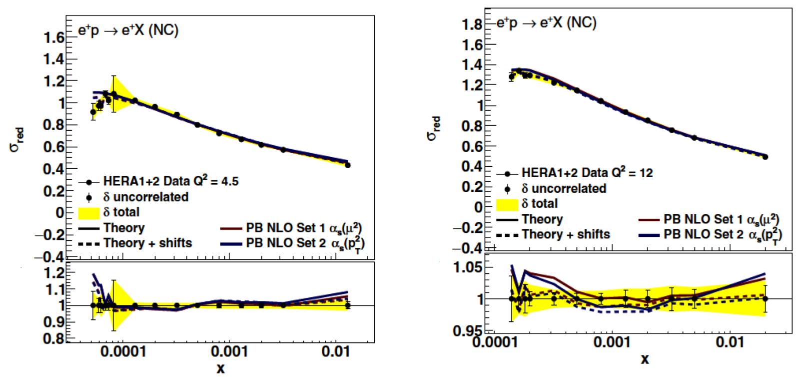

Figure 4: The reduced cross section versus x for a) $Q^2 = 4.5$ and b) 12 GeV^2 related to reference [14].

The reduced cross sections from KMR and LOMRW are similar at $Q^2 = 4.5$ GeV^2 and agree well with data at $Q^2 = 12$ GeV^2, except at very small x where the omission of F_L causes an overestimation. The PB reduced cross section matches the data closely, benefiting from fitted UPDFs.

To summarize, the KMR and LOMRW methods provide straightforward means to generate UPDFs, while the PB TMD PDFs, incorporating NLO corrections and k_t dependence from the start, offer excellent phenomenological predictions. Both the KMR and LOMRW approaches incorporate k_t and μ dependencies mainly in the final evolution step.

References

[1] V. N. Gribov and L. N. Lipatov, Yad. Fiz. 15, 781 (1972).

[2] L. N. Lipatov, Sov. J. Nucl. Phys. 20, 94 (1975).

[3] G. Altarelli and G. Parisi, Nucl. Phys. B 126, 298 (1977).

[4] Y. L. Dokshitzer, Sov. Phys. JETP 46, 641 (1977).

[5] M. A. Kimber, A. D. Martin, M. G. Ryskin, Phys. Rev. D 63, 114027 (2001).

[6] M.A. Kimber, Unintegrated parton distributions. Ph.D. thesis, University of Durham (2001).

[7] A. D. Martin, M. G. Ryskin, G. Watt, Eur. Phys. J. C 66, 163 (2010).

[8] Z. Badieian Baghsiyahi, M. Modarres, R. Kord Valeshabadi, Eur. Phys. J. C 82,392(2022).

[9] M. Modarres , R. Taghavi, R. Aminzadeh Nik, and R. Kord Valeshabadi, Phys. Rev. D 104, 056005 (2021).

[10] Ramin Kord Valeshabadi, Majid Modarres, Somayeh Rezaie, Eur. Phys. J. C 81, 961(2021).

[11] M. Modarres, R.A. Nik, R.K. Valeshbadi, H. Hosseinkhani, N. Olanj, J. Phys. G 46,105005 (2019).

[12] R. Kord Valeshabadi, M. Modarres, Eur. Phys. J. C 82, 66 (2022).

[13] R. Aminzadeh Nik, M. Modarres, N. Olanj, R. Taghavi, Phys. Rev. D 103, 074020 (2021).

[14] F. Hautmann, H. Jung, A. Lelek, V. Radescu and R. Zlebcik, JHEP **01**, 070 (2018).

[15] F. Hautmann, H. Jung, A. Lelek, V. Radescu and R. Zlebcik, Phys. Lett. B **772**, 446-451 (2017).

[16] A. Bermudez Martinez, P. Connor, H. Jung, A. Lelek, R. Zlebcik, Phys. Rev. D 99, 074008 (2019).

[17] L. A. Harland-Langa, A. D. Martinb, P. Motylinskia and R.S. Thorne, Eur. Phys. J. C 75, 204 (2015).

[18] A. Buckley, J. Ferrando and et al., Eur. Phys. J. C 75, 132 (2015).

[19] M. Modarres, M. R. Masouminia, R. Aminzadeh Nik, H. Hosseinkhani, and N. Olanj, Phys. Lett. B 772, 534 (2017).

[20] M. Modarres, R. Aminzadeh Nik, R. Kord Valeshabadi, H. Hosseinkhani, and N. Olanj, J. Phys. G 46, 105005 (2019).

[21] ZEUS and H1 Collaborations,Eur. Phys. J. C 75, 580 (2015).

[22] S. Bailey, T. Cridge, L. A. Harland-Lang, A. D. Martin and R. S. Thorne, Eur. Phys. J. C 81, 341 (2021).